Molecular Probes for Imaging Myelinated White Matter in CNS

Chunying Wu,[†] Jinjun Wei,[†] Donghua Tian,[‡] Yue Feng,[‡] Robert H. Miller,[†] and Yanming Wang*[,†]

Department of Radiology and Neurosciences, Case Western Reserve University, Cleveland, Ohio 44106, Department of Pharmacology, Emory University, Atlanta, Georgia 30322

Received March 31, 2008

Abnormalities and changes in myelination in the brain are seen in many neurodegenerative disorders such as multiple sclerosis (MS). Direct detection and quantification of myelin content in vivo is desired to facilitate diagnosis and therapeutic treatments of myelin-related diseases. The imaging studies require use of myelin-imaging agents that readily enter the brain and selectively bind to myelinated regions. For this purpose, we have systematically evaluated a series of stilbene derivatives as myelin imaging agents. Spectrophotometry-based and radioligand-based binding assays showed that these stilbene derivatives exhibited relatively high myelin-binding affinities. In vitro myelin staining exhibited that the compounds selectively stained intact myelinated regions in wild type mouse brain. In situ tissue staining demonstrated that the compounds readily entered the mouse brain and selectively labeled myelinated white matter regions. These studies suggested that these stilbene derivatives can be used as myelin-imaging probes to monitor myelin pathology in vivo.

Introduction

In both central and peripheral nervous systems, axons are insulated by myelin sheaths to facilitate efficient signal transduction of nerve impulses.[1] Myelination is one of the fundamental biological processes in biological development. Abnormalities and changes in myelination in the brain are seen in many neurodegenerative disorders such as multiple sclerosis (MS).[2,3] These changes, mainly occur in the white matter of the central nervous system (CNS)[a], are largely associated with breakdown and loss of myelin sheaths, forming demyelinated lesions.[4] The exact reasons of demyelination are still being sought. In addition, the brain has the inherent function of remyelinating in regions where myelin sheaths have been damaged.[5,6] The myelin repair process normally occurs spontaneously during the early stage of demyelination. In most myelin-related diseases, this naturally occurring process of myelin repair is hampered, resulting in the formation of demyelinated lesions.[6] Thus, therapeutic interventions are currently under development to promote and restore the remyelination process in injured brains.[7,8]

Currently, there is no direct way to quantitatively detect demyelinated lesions in vivo.[9] In clinical settings, magnetic resonance imaging (MRI) is the primary modality to assess the lesion burden in the brain.[10,11] However, any change in MR signal intensity on a dual echo T2-weighted sequence reflects a change in tissue water content, which is a nonspecific measure of the overall changes in macroscopic tissue injury, which ranges from edema, inflammation to demyelination, and axonal loss.[12] Lesions detected by MRI are not necessarily caused by demyelination. They can also be caused by other biological processes such as inflammation.[13] Thus, MRI is not a specific imaging marker for myelin and does not correlate with the degree of demyelination.

To improve the imaging specificity, various techniques have been employed such as diffusion tensor imaging, magnetic transfer imaging, etc. These MRI-related techniques, however, do not directly target at myelin membranes.[14−17] On the other hand, positron emission tomography (PET) is capable of direct characterization and quantification of biological processes at the molecular level. For myelin imaging, positron-emitting radiotracers that bind to myelin sheaths with high affinity and specificity need to be first developed. These myelin-binding probes must also penetrate the blood−brain barrier (BBB) and exhibit optimal pharmacokinetic profiles that include, among others, rapid brain uptake and high retention in myelinated regions.

Currently, lack of myelin-imaging radiotracers has limited the use of PET techniques to study myelination in vivo. To circumvent this problem, we set out to develop a series of myelin-binding agents remotely related to luxol blue. Comprehensive evaluation led us to identify two lead compounds, (*E,E*)-1,4-bis(*p*-aminostyryl)-2-methoxy-benzene (BMB)[18] and (*E,E*)-1,4-bis(4′-aminostyryl)-2-dimethoxy-benzene (BDB),[19] that readily enter the brain and selectively bind to myelined regions. In the course of our studies, we have also identified a series of stilbene derivatives that displayed promising in vitro and in situ properties for potential use of imaging of myelinated white matter. Compared to previously reported myelin-imaging probes, these compounds showed improved solubility and binding affinity. Here we report the synthesis and preliminary biological evaluation of compound 4,4′-diamino-*trans*-stilbene and its mono- and dimethylated derivatives.

Results

Chemical Synthesis. Synthesis of stilbene derivatives was achieved through Horner−Wittig reaction as shown in Scheme 1. In this study, 4-nitrobenzaldehyde and 4-dimethylamino-benzaldehyde were employed to react with a Horner−Wadsworth−Emmons reagent, (*p*-nitrobenzyl)-phosphonic acid diethyl ester (**1**), to yield (*E*)-4,4′-dinitrostilbene (**2**) and (*E*)-dimethyl-{4-[2-(4-nitro-phenyl)-vinyl]-phenyl}-amine (**5**). Further reduction

* To whom correspondence should be addressed. Phone: +1 216 844 3288. Fax: +1 216 844 8062. E-mail: yanming.wang@case.edu.

[†] Department of Radiology and Neurosciences, Case Western Reserve University.

[‡] Department of Pharmacology, Emory University.

[a] Abbreviations: MS, multiple sclerosis; MRI, magnetic resonance imaging; PET, positron emission tomography; SPECT, single photon emission computed tomography; CNS, central nervous system; BBB, blood−brain barrier; MBP, myelin basic protein; BMB, (*E,E*)-1,4-bis(*p*-aminostyryl)-2-methoxy-benzene; BDB, (*E,E*)-1,4-bis(4′-aminostyryl)-2-dimethoxy-benzene; PC, partition coefficient; HPLC, high performance liquid chromatography.

10.1021/jm8003637 CCC: $40.75
Published on Web 10/10/2008

Scheme 1[a]

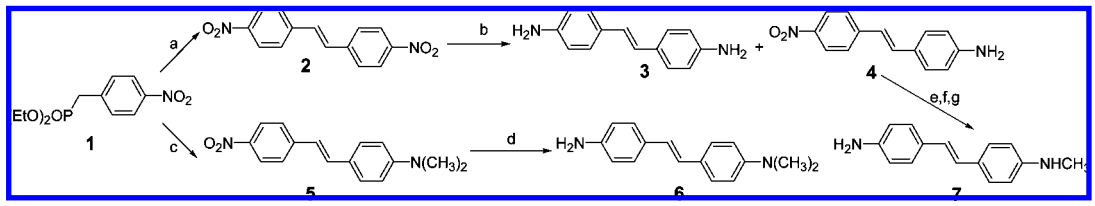

[a] (a) NaH, 4-nitrobenzaldehyde, DMF, MeOH, 83%; (b) $SnCl_2$, 1N HCl, THF; (c) 4-Dimethylamino-benzaldehyde, DMF, EtOH, $NaOCH_3$, 65%; (d) $SnCl_2$, EtOH, 64%; (e) $(CF_3CO)_2O$, Et_3N, THF; (f) (1) NaH, MeI, DMF, (2) 1N NaOH, MeOH; (g) $SnCl_2$, CH_3COOH, reflux, 35% for 4 steps.

Scheme 2[a]

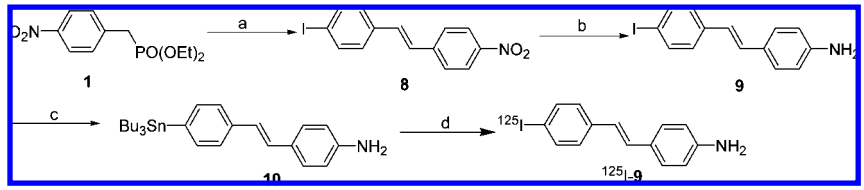

[a] (a) (1) NaH, DMF, (2) 4-iodobenzaldehyde, 2 h, 75%; (b) $SnCl_2$, EtOH, reflux, 4 h, quant; (c) $(Bu_3Sn)_2$, Et_3N, $Pd(PPh_3)_4$, 80 °C, 1 day, 60%; (d) H_2O_2, $Na^{125}I$, RT, 10 min, 70%.

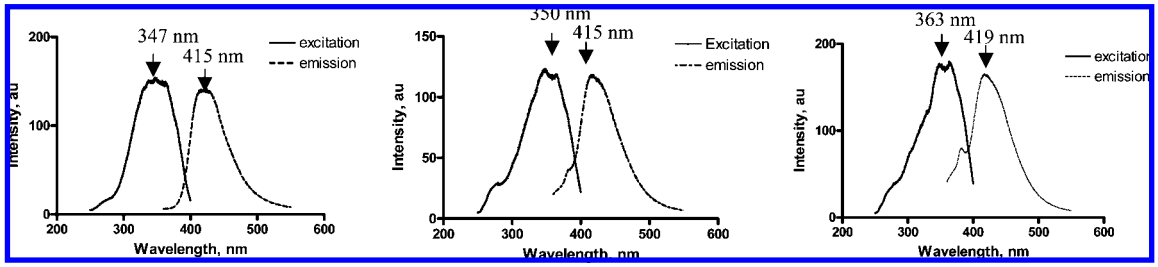

Figure 1. Excitation and emission spectra of compounds **3**, **6**, and **7** (1 μM in DMSO). Excitation spectra: emission at 415, 415, and 419 nm, range at 250−400 nm, bandwidth at 5 nm, scan at 120 nm/min, and integration time of 0.5 s, maximal excitation wavelength at 347, 350, and 363 nm. Emission spectra: excitation at 347, 350, and 363 nm, range at 360−550 nm, bandwidth at 5 nm, scan at 120 nm/min, and integration time of 0.5 s, maximal emission wavelength at 415, 415, and 419 nm.

of the nitro groups of **2** and **5** in the presence of $SnCl_2$ in ethanol furnished (*E*)-4,4′-diamino-*trans*-stilbene (**3**) and (*E*)-dimethyl-{4-[2-(4-amino-phenyl)-vinyl]-phenyl}-amine (**6**). Reduction of **2** also yielded a less polar, semireduced compound, 4-[2-(4-nitro-phenyl)-vinyl]-phenylamine (**4**), that was successfully separated and characterized by HNMR and HR-MS. Compound **4** was further protected with trifluoroacetic anhydride. Subsequently, methylation with iodomethane in the presence of potassium carbonate followed by hydrolysis and reduction yielded the monoalkylated compound, *N*-methyl-{4-[2-(4-amino-phenyl)-vinyl]-phenyl}-amine (**7**), which was purified by flash chromatography. In addition, an iodinated compound, 4-[2-(4-iodo-phenyl)-vinyl]-phenylamine (**9**) was also synthesized through Horner−Wittig reaction (see Scheme 2). 4-Iodo-benzaldehyde readily reacted with **1** in DMF in the presence of NaH. Subsequent reduction with $SnCl_2$ yielded Compound **9**. Compounds **3**, **6**, and **7** are fluorescent compounds and soluble in EtOH, CH_2Cl_2, DMSO, and other organic solvents. The excitation and emission spectra of **3**, **6**, and **7** (1 μM in DMSO), as recorded using a Cary Eclipse fluorescent spectrophotometer, are shown in Figure 1. The maximal excitation wavelengths were found at 347, 350, and 363nm, and the maximal emission wavelengths were determined at 415, 415, and 419 nm for **3**, **6**, and **7**, respectively.

Compound **9** was selected for radiolabeling with ^{125}I. The radiolabeling precursor, 4-[2-(4-tributylstannanyl-phenyl)-vinyl]-phenylamine (**10**) was first synthesized directly from the cold standard compound **9**, in which the iodo group was replaced with a tributyltin group in the presence of $Pd(PPh_3)_4$. Iododestannylation reaction using no-carrier-added sodium [^{125}I]iodide in the presence of hydrogen peroxide as the oxidant yielded [^{125}I]**9** (Scheme 2). The radiochemical identity of [^{125}I]**9** was verified by coinjection with cold standard compound **9**. Following HPLC purification, [^{125}I]**9** was obtained in 70% radiochemical yield with a radiochemical purity of >98% and a specific activity of 80 TBq/mmol. As monitored by HPLC, [^{125}I]**9** was found to be stable when kept at room temperature for up to 8 h and in the refrigerator for up to 2 months.

Spectrophotometry-Based Binding Assay. Binding affinities of newly synthesized compounds **6** and **7** were determined based on spectrophotometry. Myelin sheaths and nonmyelin pellets were extracted from rat's brain homogenates according to subcellular fraction protocol.[20] Briefly, the homogenates were successively mixed with different concentrations of sucrose and spun in a Beckman ultracentrifuge. Myelin sheaths and nonmyelin containing pellets were well separated according to their different densities and located in different layers of sucrose. The proteins were then collected and washed thoroughly with Colman buffer (10 mM). The desired proteins were aliquoted and frozen at −80 °C for up to 6 months without noticeable change in its properties, determined by electrophoresis (data not shown). Prior to binding assays, the protein fractions (myelin and pellet) were thawed and diluted with PBS (10 mM, pH 7.0). A series of concentrations of the protein fractions were incubated with tested compounds (**6** and **7**, 12.5 μM) for 1 h at room temperature. The free and bound tested compounds were then separated by centrifuging at 6000 rpm for 10 min and quantified.

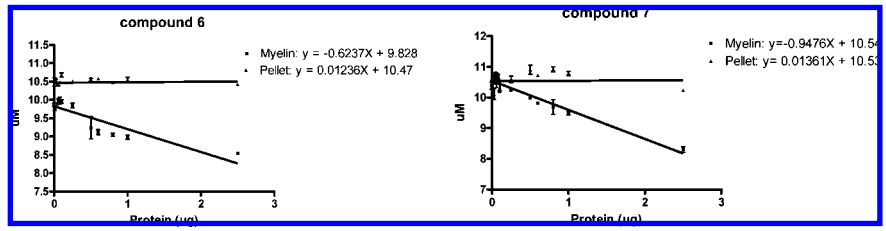

Figure 2. Correlation of the concentrations of free, unbound **6** and **7** following incubation with isolated myelin fractions and nonmyelin pellets based upon a spectroscopic assay. In these assays, 10 μM of **6** and **7** was added for each solution containing myelin fractions or nonmyelin pellets at various concentrations ranging from 0 to 2.5 μg per tube. Each data point was repeated in triplicate and an average was used.

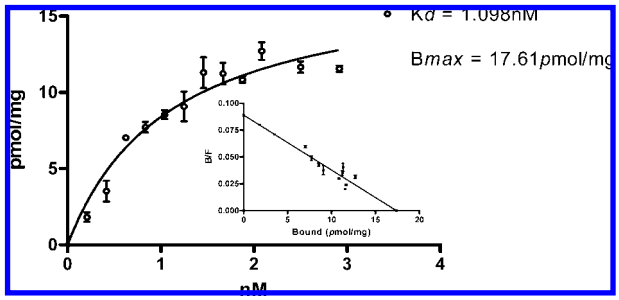

Figure 3. Saturation and scatchard plots of [^{3}H]BMB binding to isolated myelin fractions. [^{3}H]BMB displayed one-site binding. High-affinity binding with dissociation constant (K_d) values in a nanomolar range was obtained (K_d) 1.098 nM.

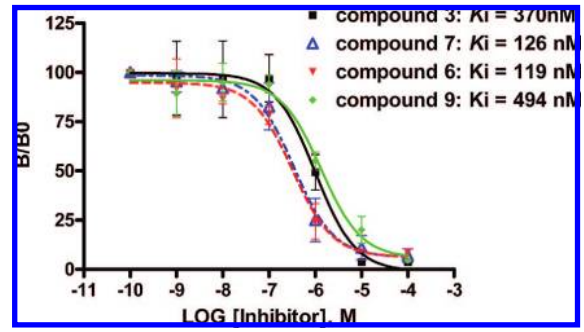

Figure 4. Competition binding assays of test compounds using [^{3}H]BMB as the radioligand in isolated myelin fractions. The concentrations that inhibited 50% of specific binding of [^{3}H]BMB (IC_{50} values) were converted to inhibition constant (K_i). K_i values were calculated using the Cheng−Prusoff equation: $K_i = IC_{50}/(1 + [L]/K_d)$, where [L] is the concentration of [^{3}H]BMB used in the assay. Data are means of three independent measurements done in duplicate.

As shown in Figure 2, when incubated with nonmyelin pellet, the concentrations of free, unbound **6** and **7** were not reduced despite the increased concentration of nonmyelin pellet. The concentrations of free **6** and **7** remained constant and close to the total concentration (10.47 μM for **6** and 10.53 μM for **7**) initially used, suggesting there was no binding to the nonmyelin fractions. In contrast, when incubated with myelin fractions, the concentrations of unbound **6** and **7** decreased proportionally when the concentrations of myelin fractions were increased, suggesting that specific binding interactions exist between the test compounds and the myelin fractions.

Radioligand-Based Binding Assays. In vitro binding assay using radioligand is the most sensitive techniques available to quantitatively determine the binding affinities of compounds to certain proteins. Our previous studies have shown that BMB binds to myelin sheaths with high affinity and specifity.[18] For this reason, tritiated BMB was custom synthesized by American Radiolabeled Chemicals Inc. (St Louis, MO) and was used as the radioligand for binding assays. This allowed us to determine the binding affinities of the newly synthesized compounds using isolated rat myelin fractions. Saturation experiment was first conducted using [^{3}H]BMB. As shown in Figure 3, [^{3}H]BMB displayed saturable binding with isolated myelin fractions of rats and approximately 30% of [^{3}H]BMB binding to isolated rat myelin was displaced by 1.0 μM unlabeled BMB. Transformation of the saturation binding of [^{3}H]BMB to Scatchard plots gave linear plots, suggesting that it involved a single population of binding sites (Figure 3). The dissociation constant (K_d value) was 1.098 ± 0.20 nM and B_{max} value was 17.61 *p*mol/mg under the assay condition, respectively. Competitive binding assays were also conducted using [^{3}H]BMB as radioligand. The stilbene derivatives competed effectively with [^{3}H]BMB binding sites on rat myelin fractions at affinities of low micromole concentrations. As shown in Figure 4, the K_i values estimated for **3**, **6**, **7**, and **9** were 370, 119, 126, and 494 nM, respectively. These K_i values suggested that all these derivatives of stilbene had relatively high binding affinity for myelin fractions in the order of **7** > **6** > **3** > **9**.

In Vitro Staining of Myelinated White Matter. We then evaluated the myelin-binding properties of the newly synthesized compounds **3**, **6**, and **7** through in vitro staining of mouse brain tissue sections. Both myelinated corpus callosum and cerebellar regions were then examined by fluorescent microscopy. At 10 μM concentration, compounds **3**, **6**, and **7** selectively labeled both corpus callosum and cerebellum (Figure 5), exhibiting staining patterns that were virtually identical to the pattern observed in immunohistochemical staining of MBP.[19]

In Situ Tissue Staining of Myelinated White Matter. Following our in vitro tissue staining studies, we then evaluated the brain permeability and subsequent myelin-binding properties of **6** and **7** in the mouse brain. A dose of **6** or **7** (20−80 mg/kg) was administered via tail vein injection into wild-type mice. Three hours post injection, the mouse brains were perfused with saline followed by 4% paraformaldehyde (PFA) and removed. The fresh frozen brains were then sectioned. Fluorescent staining of myelinated regions such as the cerebellum were then directly examined under a microscope. As shown in Figure 6, fluorescent compounds **6** and **7** readily entered the mouse brain and selectively labeled myelinated cerebellum.

Partition Coefficient. The partition coefficient (PC) is an important parameter of brain permeability. PC values ranging from 1.0 to 3.5 often show good initial brain entry following iv injection.[21−23] For this reason, we radioiodinated compound **9** and quantitatively determined the lipophilicity of [^{125}I]**9**. On the basis of the conventional octanol−water partition measurement, the logPoct of [^{125}I]**9** was determined as 2.5 ± 0.1, which falls in the range for optimal brain entry.

Permeability across the Blood−Brain Barrier in Mice. Encouraged by the aforementioned studies, we further evaluated the permeability of [^{125}I]**9** across the blood−brain barrier. Following bolus tail vein injection of [^{125}I]**9** (0.2 mL, 0.185 MBq), the radioactivity concentration of [^{125}I]**9** in the brain was

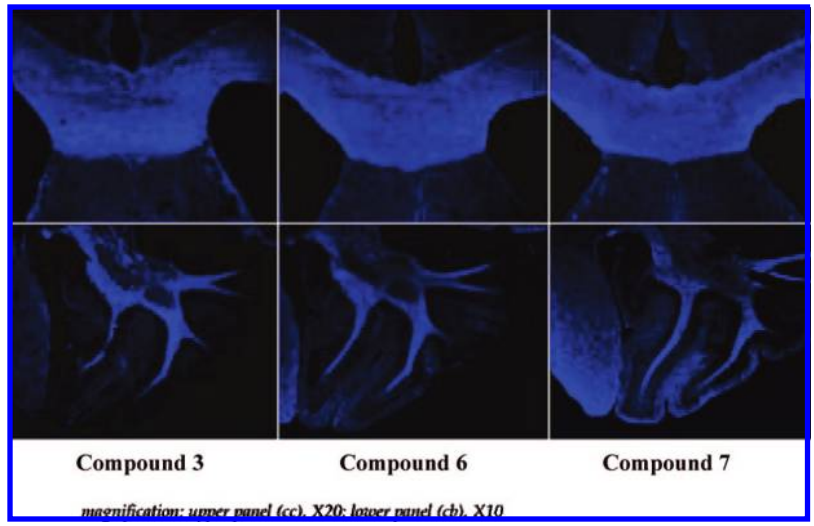

Figure 5. In vitro staining of corpus callosum (top) and cerebellum (bottom) in wild-type mouse brain.

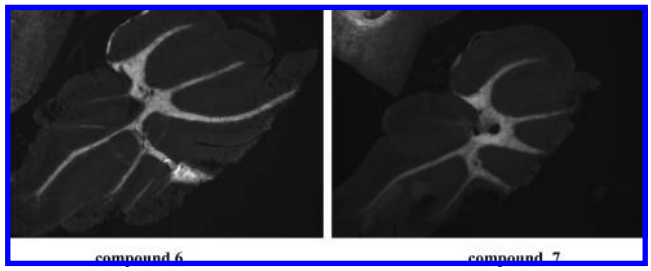

Figure 6. In situ staining of myelin sheaths in the cerebellum of mouse brain.

Table 1. Brain Uptake of ^{125}I-**9** in Mice ($n = 3$, %ID/g)

organ	2 min	30 min	60 min	120 min
brain	2.29 ± 0.66	2.65 ± 0.27	2.05 ± 0.13	1.12 ± 0.23

determined at 2, 30, and 60 min post injection. As shown in Table 1, [^{125}I]**9** displayed rapid brain entry at early time intervals. The initial brain entry was 2.29 ± 0.66% ID/g at 2 min post injection. At 30 min post injection, the brain radioactivity concentration reached its peak level (2.65 ± 0.27% ID/g). The radioactivity concentration slowly decreased to 1.12 ± 0.23% ID/g at 120 min post injection. These results indicated that [^{125}I]**9** readily entered the brain. Retention of [^{125}I] **9** at later time points was likely due to binding to myelin membranes as indicated by aforementioned in vitro and in situ staining studies.

Autoradiography in Mice. To further evaluate the binding specificity of [^{125}I]**9** to myelin sheaths in the brain, in vitro autoradiography was carried out in mice. As shown in Figure 7, a distinct labeling of myelinated regions such as corpus callosum and cerebellum were observed after the mouse brain tissue sections (sagittal) were exposed to [^{125}I]**9**. The result indicated that the autoradiographic visualization was consistent with the histological staining of myelinated regions (i.e., corpus callosum and cerebellum).

Discussion

The results showed that the myelin-binding probes readily enter the brain and selectively bound to myelin sheaths. It is worth note that the myelin-imaging probes are not designed to detect individual myelin fibers nor single lesions but to determine the abundance of myelin membranes in selected

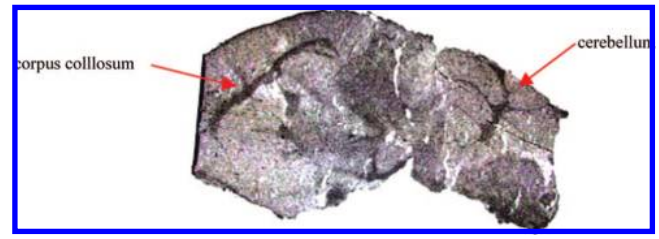

Figure 7. Film autoradiography shows [^{125}I] **9** binding to myelinated corpus collosum and cerebellum in mouse brain sections (sagittal). Arrows show myelinated corpus collosum (A) and cerebellum (B) labeled by [^{125}I]**9**.

regions of interest. The myelin abundance can be determined through imaging studies by the retention of radiotracers in terms of radioactivity concentration in myelinated brain regions. Similarly, the myelin abundance can also be determined in brain regions containing demyelinated lesions, which is expected to be lower than that in the normally myelinated regions. The lesion profiles are heterogenic based on analysis of a large pathology sample of multiple sclerosis patients (MS).[24] One of the key diagnostic criteria in MS is the presence of demyelinated lesions of 5 mm in size. This size is well above the resolution limits of nuclear imaging modalities. Thus, it is very feasible to accurately determine the myelin abundance in terms of radioactivity concentration of the radiotracers in demyelinated regions.

In practice, both MRI and PET or single photon emission computed tomography (SPECT) will be conducted. MRI is used to provide anatomical information of the brain in order to define regions of interest. Following MRI, PET or SPECT will be conducted and coregistered with MRI images to determine radioactivity concentration in defined regions of interest.

During our in situ staining studies, we used a dose ranging from 20−80 mg/kg. The mice all survived very well without any pharmacological effects observed. Following removal of the brain, we also examine various organs in the other part of the body and did not observe any abnormality in liver, lung, spleen, or kidney. These studies suggested that there is no toxic effect below 80 mg/kg. For imaging studies, the concentration of the radiotracers used will be in nanomolar concentration or at least 1000 times lower than the dose we used in the staining studies. Therefore, no toxicity effect should be expected.

Finally, these compounds do not dissolve in myelin membranes but likely bind to myelin through direct and specific

interactions with MBP. The binding mechanism is not known but our previous work with structurally related myelin-imaging probes indicated that they bind to pleated β-sheet structure present in myelin basic protein (MBP).[18]

Conclusion

Several stilbene derivatives have been synthesized and evaluated for potential in vivo imaging of myelinated brain regions. These small molecular probes selectively stain myelinated white matter regions such as the corpus callosum and cerebellum in mouse brain tissue sections. The white matter staining was also achieved in situ following tail vein injections, suggesting they readily enter the brain. Both spectrophotometry and radioligand-based binding assays suggested a specific interaction of these compounds with myelin membranes. These in vitro and in situ binding properties, coupled with its permeability across the BBB, make them promising candidates for further investigation as in vivo myelin-imaging agents.

Methods and Materials

1. Synthesis. 1.1. Synthesis of 4,4′-Dinitro-*trans*-stilbene (2). Under Ar, (4-nitro-benzyl)-phosphoric acid diethyl ester (**1**, 1.81 g, 6.6 mmol) and 4-nitrobenzaldehyde (1.00 g, 6.6 mmol) were dissolved in DMF (10 mL) and EtOH (10 mL). Then $NaOCH_3$ (2.3 mL, 4.37 M) in MeOH was added and the suspension was stirred for another 3 h. The solid was filtered and dried in vacuum to give 1.50 g (yield: 83%) of 4,4′-dinitro-*trans*-stilbene. ^{1}H NMR (300 MHz, $CDCl_3$): 8.28 (d, J = 8.4 Hz, 4 H), 7.94 (d, J = 8.4 Hz, 4 H), 7.69 (s, 2 H).

1.2. Synthesis of 4,4′-Diamino-*trans*-stilbene (3) and 4-[2-(4-Nitro-phenyl)-vinyl]-phenylamine (4). To a solution of compound **2** (0.10 g, 0.4mmol) in THF (20 mL) was added $SnCl_2$ (1.50 g) dissolved in 1N HCl (10 mL). The reaction mixture was stirred overnight at room temperature. The acidic solution was then neutralized using 1N NaOH and extracted with ethyl acetate (3 × 20 mL). The combined organic phases were washed with water and brine, dried over Na_2SO_4, and concentrated. Purification with flash column (HE:EA = 2:1 to 1:1) yielded 4,4′-diamino-*trans*-stilbene (**3**, 0.03 g, 40%) and 4-[2-(4-nitro-phenyl)-vinyl]-phenylamine (**4**). ^{1}H NMR of **3** (300 MHz, $CDCl_3$): 7.31 (d, J = 8.4 Hz, 4 H), 6.86 (s, 2 H), 6.68 (d, J = 8.4 Hz, 4 H). HR-ESIMS of **3**: m/z calcd for $C_{14}H_{14}N_2$ ($M + H^+$): 211.1230, found 211.1225. Melting point of **3**: 206.1−207.3 °C. ^{1}H NMR of **4** (300 MHz, $CDCl_3$): 8.22 (d, J = 8.0 Hz, 2 H), 7.59 (d, J = 6.86 Hz, 2 H), 7.41 (d, J = 8.57 Hz, 4 H), 7.22 (d, J = 17.14 Hz, 1 H), 6.97 (d, J = 12.57 Hz, 1 H), 6.72 (d, J = 10 Hz, 2 H).

1.3. Synthesis of Dimethyl-{4-[2-(4-nitro-phenyl)-vinyl]-phenyl}-amine (5). To a solution of 4-dimethylamino-benzaldehyde (2.24 g, 15 mmol) and (4-nitro-benzyl)-phosphoric acid diethyl ester (**1**, 4.10 g, 15 mmol) in DMF (20 mL) and EtOH (20 mL) was added to $NaOCH_3$ (1.62 g, 30 mmol). The suspension was stirred and refluxed for 3 h. After cooled to room temperature, the precipitate was filtered and washed thoroughly with ethanol to give dimethyl-{4-[2-(4-nitro-phenyl)-vinyl]-phenyl}-amine (**5**, 2.55 g, 65%) as red solid. **5** was used without further purification.

1.4. Synthesis of Dimethyl-{4-[2-(4-amino-phenyl)-vinyl]-phenyl}-amine (6). To a solution of **5** (2.55 g, 9.5mmol) in EtOH (100 mL) was added to $SnCl_2$ (8.58 g, 38 mmol). The resulting mixture was refluxed for 4 h. The solvent was then removed under vacuum and NaOH (2 mol/L, 40 mL) was added to the residue. The crude solid was filtered and suspended in ethyl acetate (200 mL). The precipitates were then filtered to give dimethyl-{4-[2-(4-amino-phenyl)-vinyl]-phenyl}-amine (**6**, 1.45 g, 64%) as gray solid. ^{1}H NMR (300 MHz, $CDCl_3$): 7.40 (d, J = 8.62 Hz, 2 H), 7.33 (d, J = 8.40 Hz,2 H), 6.86 (d, J = 5.92 Hz, 2 H), 6.76 (d, J = 8.34 Hz, 2 H), 6.69 (d, J = 8.22 Hz, 2 H), 2.99 (s, 6 H). HR-ESIMS: m/z calcd for $C_{16}H_{18}N_2$ ($M + H^+$), 239.1543; found, 239.1542. Melting point: 167.7−168.5 °C.

1.5. Synthesis of *N*-Methyl-{4-[2-(4-amino-phenyl)-vinyl]-phenyl}-amine (7). To a solution of **4** (50 mg, 2 mmol) dissolved in THF (5 mL) under argon was added to Et_3N (1 mL). The solution was stirred for 4 h. The solvent was evaporated under vacuum, and the protected product was then used without further purification.

To the solution of the above protected product dissolved in DMF (5 mL) were added NaH (0.10 g) and iodomethane (1 mL). The vial was sealed and stirred overnight. Then the solution was diluted with methanol (8 mL) and 1 M NaOH solution (2 mL). After stirred for another 2 h, the solution was extracted with ethyl acetate. The combined organic layer was washed with water and brine and dried over Na_2SO_4. Following concentration, the reduced product was then subsequently used without further purification.

To the suspension of the above compound in acetic acid (10 mL) was added tin(II) chloride (1.0 g). The suspension was heated to reflux for 2 h. After concentration, the residue was dissolved in ethyl acetate, washed with 2N NaOH solution, water, and brine. Dried over Na_2SO_4, the solution was concentrated and purified by flash column (hexanes:ethyl acetate = 2:1 to 1:1) to give 15 mg of **7** (0.6 mmol, 35% yield for the above three steps). ^{1}H NMR (400 MHz, $CDCl_3$): 7.36 (d, J = 8.3 Hz, 2 H), 7.32 (d, J = 8.2 Hz, 2 H), 6.87 (AB, J = 18.7 Hz, 16.5 Hz, 2 H), 6.69 (d, J = 8.2 Hz, 2 H), 6.62 (d, J = 8.3 Hz, 2 H), 3.92 (br, 3 H), 2.88 (s, 2 H). HR-ESIMS: m/z calcd for $C_{15}H_{16}N_2$ ($M + H^+$), 225.1386; found, 225.1385. Melting point: 143.7−144.7 °C.

1.6. Synthesis of 4-Amino-4′-iodostilbene (8). To a solution of diethyl 4-nitrobenzylphosphate (0.44 g, 1.61 mmol) dissolved in DMF (10 mL) was added NaH (0.07 g, 1.75 mmol). The suspension was stirred for 1 h followed by addition of 4-iodobenzaldehyde (0.35 g, 1.51 mmol). The suspension was stirred for another 2 h. Water was added and the solid was collected by filtration to give **8** (0.40 g, 1.14 mmol, yield: 75%). ^{1}H NMR (400 MHz, $CDCl_3$): 8.24 (d, J = 8.65 Hz, 2 H), 7.88 (d, J = 8.68 Hz, 2 H), 7.80 (d, J = 8.19 Hz, 2 H), 7.49 (m, J = 8.2 Hz, 4 H).

1.7. Synthesis of 4-[2-(4-Iodo-phenyl)-vinyl]-phenylamine (9). To a suspension of compound **8** (0.20 g, 0.57 mmol) in ethanol (10 mL) was added Tin(II) chloride (1.00 g, 5 mmol) and heated to reflux for 4 h under argon. The ethanol was evaporated under vacuum. The residue was dissolved in ethyl acetate, washed with 1N NaOH, water, and brine. Dried over Na_2SO_4, the solution was concentrated and purified by flash column (hexanes:ethyl acetate = 2:1 to 1:1) to give **9** (0.18 g, quant. yield). ^{1}H NMR (400 MHz, $CDCl_3$): 7.66 (d, J = 8.25 Hz, 2 H), 7.35 (d, J = 8.34 Hz, 2 H), 7.04 (d, J = 15.73 Hz, 1 H), 6.71 (d, J = 16.26 Hz, 1 H), 6.70 (d, J = 8.29 Hz, 2 H). HR-ESIMS: m/z calcd for $C_{14}H_{12}IN$ ($M + H^+$), 322.0087; found, 322.0084. Melting point: 213.4−215.2 °C.

1.8. Synthesis of 4-[2-(4-Tributylstannanyl-phenyl)-vinyl]-phenylamine (10). Under Ar, the substrate **9** (0.05 g, 0.15 mmol) was mixed with $(Bu_3Sn)_2$ (1 mL), $Pd(PPh_3)_4$ (0.02 g), and Et_3N (5 mL). The mixture was sealed in a vial and heated to 80 °C for 1 day. The solvent was evaporated in vacuum, and the residue was purified by column to give **10** (44 mg, 0.09 mmol, yield: 60%). ^{1}H NMR (400 MHz, $CDCl_3$): 7.42 (s, 4 H), 7.33 (d, J = 7.87 Hz, 2 H), 7.03 (d, J = 16.18 Hz, 1 H), 6.89 (d, J = 16.24 Hz, 1 H), 6.66 (d, J = 8.08 Hz, 2 H), 1.55 (m, 6 H), 1.34 (m, 6 H), 1.05 (t, 6 H), 0.89 (t, 9 H).

1.9. Radiosynthesis of 4-[2-(4-[^{125}I]Iodo-phenyl)-vinyl]-phenylamine ([^{125}I]9). To a sealed vial were added **10** (50 μL, 50 μg in 50 μL of ethanol), [^{125}I] sodium iodide, and 1N HCl (100 μL). Subsequently, 100 μL of H_2O_2 (3%, in water) was added via a syringe at room temperature. After 10 min, the iodination reaction was terminated by an addition of saturated $NaHSO_3$, and the resulting solution was neutralized to pH 7−8 by adding a saturated $NaHCO_3$ solution. The mixture was extracted with ethyl acetate (3 × 1 mL). The combined organic layers were dried over Na_2SO_4, and the solvent was removed by a stream of dry nitrogen gas. The residue was purified by high performance liquid chromatography (HPLC; C-18 column; acetonitrile; DMGA (5 mM, pH 7.4): 60/40; flow rate: 1 mL/min; retention time: 21 min) to get 18.5 MBq of final pure product with radiochemical purity over 98% and a

specific activity near the theoretical limit (80 TBq/mmol). The chemical identity was verified by coinjection of the "cold standard" (nonradioactive compound).

2. Partition Coefficients. Partition coefficients (PC) were measured by mixing the radioligands with 3 g (3.65 mL) of 1-octanol and 3 g (3.0 mL) of buffer (pH 7.40, 0.1 M phosphate) in a test tube. The test tube was vortexed for 3 min at room temperature and then centrifuged (3500 rpm, 5 min). 1 mL of samples from the 1-octanol and buffer layers were assayed for radioactivity content in a well γcounter. The partition coefficient was determined by calculating the ratio of cpm/g of 1-octanol to that of the buffer. Samples from the 1-octanol layer were repartitioned until consistent partitions of coefficient values were obtained. The measurement was repeated at least three times. PC was 2.5 ± 0.1 at pH 7.40.

3. Brain Uptake of [^{125}I]9. While under anesthesia, 0.1 mL of a saline solution (consisting of saline (2 mL, 9 mg/mL), propylene glycol (2 mL), ethanol (0.7 mL), and HCl (0.3 mL, 0.3 nM)),[25] containing 5 μCi of radioactive tracer, was injected into the tail veins of mice (Swiss−Webster, 2 month old, 2 mice per group). The mice were sacrificed by heart puncture at 2, 30, 60, and 120 min post injection under anesthesia. Brains were rapidly removed and weighed, and the brain uptake was expressed as percentage of injection dose per gram organ (%ID/g), which was calculated by a ratio of per gram tissue counts to counts of 1% of the initial dose (100 times diluted aliquots of the injected radioligand) measured at the same time.

4. In Vitro Autoradiography of [^{125}I]9. Mouse brain sections were incubated in [^{125}I]**9** (20% ethanol, 4380000 cpm/16 mL) for 1 h. The slides were quickly washed with PBS buffer (10 mM, pH 7.0) 3 times, saturated Li_2CO_3 in 40% ethanol (2 × 3 min), 40% ethanol (2 min), and H_2O (30 s). After drying by air, the slides were put in a cassette and exposed to film for 44 h to obtain images.

5. In Vitro Tissue Staining of Normal Control Mice Brain Section. Normal control mice were deeply anesthetized and perfused transcardially with saline (10 mL) followed by fixation with 4% PFA in PBS (10 mL, 4°æ, pH 7.6). Brain tissues were then removed, postfixed by immersion in 4% PFA overnight, dehydrated in 30% sucrose solution, embedded in freezing compound (OCT, Fisher Scientific, Suwanee, GA), cryostat sectioned at 10 μm on a microtome, and mounted on superfrost slides (Fisher Scientific). The brain sections were incubated with compound **3**, **6**, and **7** (10 μM, 1% DMSO in PBS (10 mM, pH 7.0)) for 20 min at room temperature in dark. Excess compounds were washed by briefly rinsing the slides in PBS (10 mM, pH 7.0) and coverslipped with fluoromount-G mounting media (Vector Laboratories, Burlingame, CA). Sections were then examined under an IX51 fluorescent microscope.

6. In Situ Tissue Staining of Normal Control Mice Brain Section. Under anesthesia, wild-type mice were injected with compounds **6** and **7** (20−80 mg/kg) via the tail vein, and the mice were then perfused transcardially with saline (10 mL) followed by 4% PFA in PBS (10 mL, 4 °C, pH 7.6). Brain tissues were then removed, postfixed by immersion in 4% PFA overnight, dehydrated in 30% sucrose solution, cryostat sectioned at 16 μm on a microtome and mounted on superfrost slides (Fisher Scientific), and imaged directly under fluorescent microscopy without any further staining.

7. Extraction of Myelin Fractions. Sprague−Dawley (SD) rats were asphyxiated with CO_2. When the rat had stopped breathing, the skin/fur over the neck was wetted with a spray of 70% ethanol. The brains were then taken out and put into 0.32 mol/L sucrose (1 × Colman buffer) in the homogenizer, first with the loose pestle 5−8 times and then with the tight pestle until the solution reached a uniform consistency. The solution was then transferred from the homogenizer to the corresponding tubes. The tubes were centrifuged at 1000 rpm (4 °C) for 10 min. The resulting supernatant was carefully removed and transferred into Beckmann tubes that were previously filled with 2.80 mol/L sucrose and mixed thoroughly. After carefully overlaying nearly to the top of the tube with 0.25 mol/L sucrose, the tube was spun in the Beckman ultracentrifuge for 2.5 h at 35000 rpm (4 °C). The 0.25 mol/L sucrose layer was drawn off and discarded. The myelin fraction was collected at the 0.25 mol/L and 0.85 mol/L sucrose interface, and the pellet was collected at the 0.85 mol/L and /1.4 mol/L sucrose interface. Both myelin and pellet were washed with buffer (1 × colman, 7−8 mL) three times before being suspended in buffer (1 × colman, 5 mL) and kept in −80 °C freezer for future use. The concentration of myelin and pellet were determined by Bio-Rad Protein Assay.

8. Spectrophotometry-Based Binding Assays. In the spectrophotometry-based binding assays, a solution of **6** or **7** (800 μL, 12.5 μM) dissolved in 10% DMSO buffer solution containing 10 mM $MgCl_2$ and 10 mM PBS (pH 7.4) was incubated with isolated myelin or pellets at different concentrations ranging from 0.06 to 14 μg/tube. Each tube contained 10 μM of **6** or **7**, 10% DMSO buffer, and membrane fraction in a final volume of 1 mL. Following incubation at room temperature for 1 h, the free and bound **6** or **7** was separated by centrifugation at 6000 rpm for 10 min. The supernatant was then collected and the UV absorption of free **6** or **7** determined by UV spectrometer were at 350 or 363 nm. The concentration of free **6** or **7** was obtained by comparison to a standard curve. In parallel, nonspecific binding was determined using pellets under the same condition. All assays were performed in triplicate.

9. Radioligand-Based Binding Assays. The radioligand-based binding assays were carried out in 12 mm × 75 mm borosilicate glass tubes. For saturation studies, the reaction mixture contained 50 μL of myelin fraction (1−2 μg, 1 × PBS), 50 μL of [^{3}H]BMB (diluted in 1 × PBS, 0.25−3.5 nM) in a final volume of 500 μL. Nonspecific binding was defined in the presence of cold BMB (1 μM, diluted in PBS (containing 1‰ DMSO) in the same assay tubes. For the competition binding, 10^{-5} to 10^{-10} M compounds and 1.87 nM [^{3}H]BMB were used for the studies. The mixture was incubated at 37 °C for 2 h. The bound and free radioactivity were separated by rapid vacuum filtration through Whatman GF/B filters using a Brandel M-24R cell harvester followed by 3 × 2 mL washes of PBS at room temperature. Filters containing the bound radioligand were dissolved in 6 mL of biodegradable counting cocktail overnight and the radioactivity was assayed the next day in the scintillation counter (Beckman) with 42% counting efficiency. The results of saturation and inhibition experiments were subjected to nonlinear regression analysis using Graph Pad Prism 4 by which K_d and K_i values were calculated.

Acknowledgment. We gratefully acknowledge the support from the Myelin Repair Foundation, the Dana Foundation, National Multiple Sclerosis Society, and National Institute of Neurodegenerative Disorders and Stroke (NS054109, NS061837, and NS30800). We also thank Norbert Owino for reproduction of some of the compounds and Eduardo Somoza for assistance in preparation of the manuscript.

Supporting Information Available: A table listing the appropriate analytical data including melting points, spectrum of HPLC, HRMS, and ^{1}HNMR for determining degree of purity for compounds **3**, **6**, **7**, and **9**. This material is available free of charge via the Internet at http://pubs.acs.org.

References

(1) Morell, P.; Quarles RH In Basic Neurochemistry: Molecular, Cellular, and Medical Aspects. *Myelin Formation, Structure, and Biochemistry*, 6th ed.; Lippincott-Raven: Philadelphia, 1999; pp 79−93.
(2) Compston, A.; Coles, A. Multiple sclerosis. *Lancet* **2002**, *359*, 1221–1231.
(3) McFarlandH. McFarlinD. Immunologicallly mediated demyelinating diseases of the central and peripheral nervous system. In *Immunologic Diseases*; Little Brown: Boston, 1995; pp10811101.
(4) Miller, D. J.; Asakura, K.; Rodriguez, M. Central nervous system remyelination clinical application of basic neuroscience principles. *Brain Pathol.* **1996**, *6*, 331–344.
(5) Perier, O.; Gregoire, A. Electron microscopic features of multiple sclerosis lesions. *Brain* **1965**, *88*, 937–952.

(6) Trapp, B. D.; Peterson, J.; Ransohoff, R. M.; Rudick, R.; Mork, S.; et al. Axonal transection in the lesions of multiple sclerosis. *N. Engl. J. Med.* **1998**, *338*, 278–285.

(7) McMorris, F. A.; McKinnon, R. D. Regulation of oligodendrocyte development and CNS myelination by growth factors: prospects for therapy of demyelinating disease. *Brain Pathol.* **1996**, *6*, 313–329.

(8) Duncan, I. D. Glial cell transplantation and remyelination of the central nervous system. *Neuropathol. Appl. Neurobiol.* **1996**, *22*, 87–100.

(9) Stangel, M. Transplantation of myelinating cells as regenerative therapy for multiple sclerosis - experimental basis and present state of clinical studies. *Nervenarzt* **2002**, *73*, 937–945.

(10) McDonald, W. I.; Compston, A.; Edan, G.; Goodkin, D.; Hartung, H. P.; et al. Recommended diagnostic criteria for multiple sclerosis: guidelines from the International Panel on the diagnosis of multiple sclerosis. *Ann. Neurol.* **2001**, *50*, 121–127.

(11) Polman, C. H.; Reingold, S. C.; Edan, G.; Filippi, M.; Hartung, H. P.; et al. Diagnostic criteria for multiple sclerosis: 2005 revisions to the "McDonald Criteria". *Ann. Neurol.* **2005**, *58*, 840–846.

(12) Filippi, M.; Falini, A.; Arnold, D. L.; Fazekas, F.; Gonen, O.; et al. Magnetic resonance techniques for the in vivo assessment of multiple sclerosis pathology: consensus report of the white matter study group. *J. Magn. Reson. Imaging* **2005**, *21*, 669–675.

(13) Owens, T. The enigma of multiple sclerosis: inflammation and neurodegeneration cause heterogeneous dysfunction and damage. *Curr. Opin. Neurol.* **2003**, *16*, 259–265.

(14) Guttmann, C. R.; Meier, D. S.; Holland, C. M. Can MRI reveal phenotypes of multiple sclerosis. *Magn. Reson. Imaging* **2006**, *24*, 475–481.

(15) Bitsch, A.; Bruhn, H.; Vougioukas, V.; Stringaris, A.; Lassmann, H.; et al. Inflammatory CNS demyelination: histopathologic correlation with in vivo quantitative proton MR spectroscopy. *AJNR Am. J. Neuroradiol.* **1999**, *20*, 1619–1627.

(16) Ropele, S.; Strasser-Fuchs, S.; Augustin, M.; Stollberger, R.; Enzinger, C.; et al. A comparison of magnetization transfer ratio, magnetization transfer rate, and the native relaxation time of water protons related to relapsing-remitting multiple sclerosis. *AJNR Am. J. Neuroradiol.* **2000**, *21*, 1885–1891.

(17) Goldberg-Zimring, D.; Mewes, A. U.; Maddah, M.; Warfield, S. K. Diffusion tensor magnetic resonance imaging in multiple sclerosis. *J. Neuroimaging* **2005**, *15*, 68S–81S.

(18) Stankoff, B.; Wang, Y.; Bottlaender, M.; Aigrot, M. S.; Dolle, F.; et al. Imaging of CNS myelin by positron-emission tomography. *Proc. Natl. Acad. Sci. U.S.A.* **2006**, *103*, 9304–9309.

(19) Wu, C.; Tian, D.; Feng, Y.; Polak, P.; Wei, J.; et al. A novel fluorescent probe that is brain permeable and selectively binds to myelin. *J. Histochem. Cytochem.* **2006**, *54*, 997–1004.

(20) Martenson, R. E.; Deibler, G. E.; Kies, M. W. Extraction of rat myelin basic protein free of other basic proteins of whole central nervous system tissue. An analysis of its electrophoretic heterogeneity. *J. Biol. Chem.* **1969**, *244*, 4268–4272.

(21) Wu, C.; Pike, V. W.; Wang, Y. Amyloid imaging: from benchtop to bedside. *Curr. Top. Dev. Biol.* **2005**, *70*, 171–213.

(22) Levin, V. A. Relationship of octanol/water partition coefficient and molecular weight to rat brain capillary permeability. *J. Med. Chem.* **1980**, *23*, 682–684.

(23) Dishino, D. D.; Welch, M. J.; Kilbourn, M. R.; Raichle, M. E. Relationship between lipophilicity and brain extraction of C-11-labeled radiopharmaceuticals. *J. Nucl. Med.* **1983**, *24*, 1030–1038.

(24) Lucchinetti, C.; Bruck, W.; Parisi, J.; Scheithauer, B.; Rodriguez, M.; et al. Heterogeneity of multiple sclerosis lesions: implications for the pathogenesis of demyelination. *Ann. Neurol.* **2000**, *47*, 707–717.

(25) Aboofazeli, R.; Zia, H.; Needham, T. E. Transdermal delivery of nicardipine: an approach to in vitro permeation enhancement. *Drug Delivery* **2002**, *9*, 239–247.

JM8003637